Nanozyme-mediated catalytic nanotherapy for inflammatory bowel disease

Jiulong Zhao,[1,2‡] Wei Gao,[3‡] Xiaojun Cai,[1,3,*] Jiajia Xu[2], Duowu Zou,[2,*] Zhaoshen Li,[2] Bing Hu,[3,*] Yuanyi Zheng,[1,*]

[1]Shanghai Institute of Ultrasound in Medicine, Shanghai Jiao Tong University Affiliated Sixth People's Hospital, Shanghai 200233 (China)

[2]Department of Gastroenterology, Changhai Hospital, Second Military Medical University, Shanghai 200433 (China)

[3]Department of Ultrasound in Medicine, Shanghai Jiao Tong University Affiliated Sixth People's Hospital, Shanghai 200233 (China)

*Corresponding authors: Dr. Xiaojun Cai, c1x2j34@163.com; Prof. Duowu Zou, zdw_pi@163.com; Prof. Bing Hu, binghu_stephen@163.com; Prof. Yuanyi Zheng, zhengyuanyi@163.com;

‡These authors contributed equally to this work.

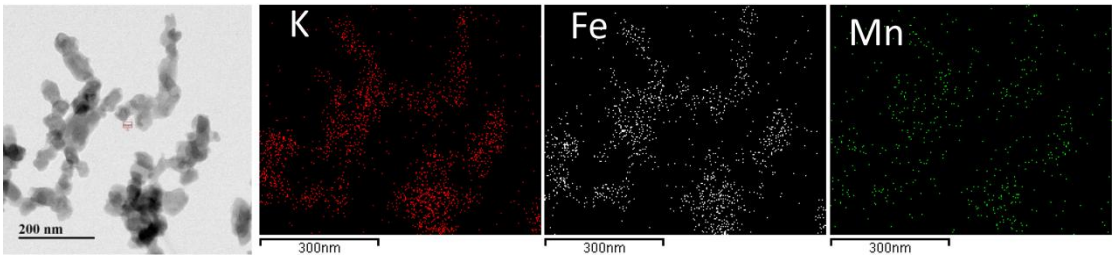

Figure S1. The element mapping of MPBZs

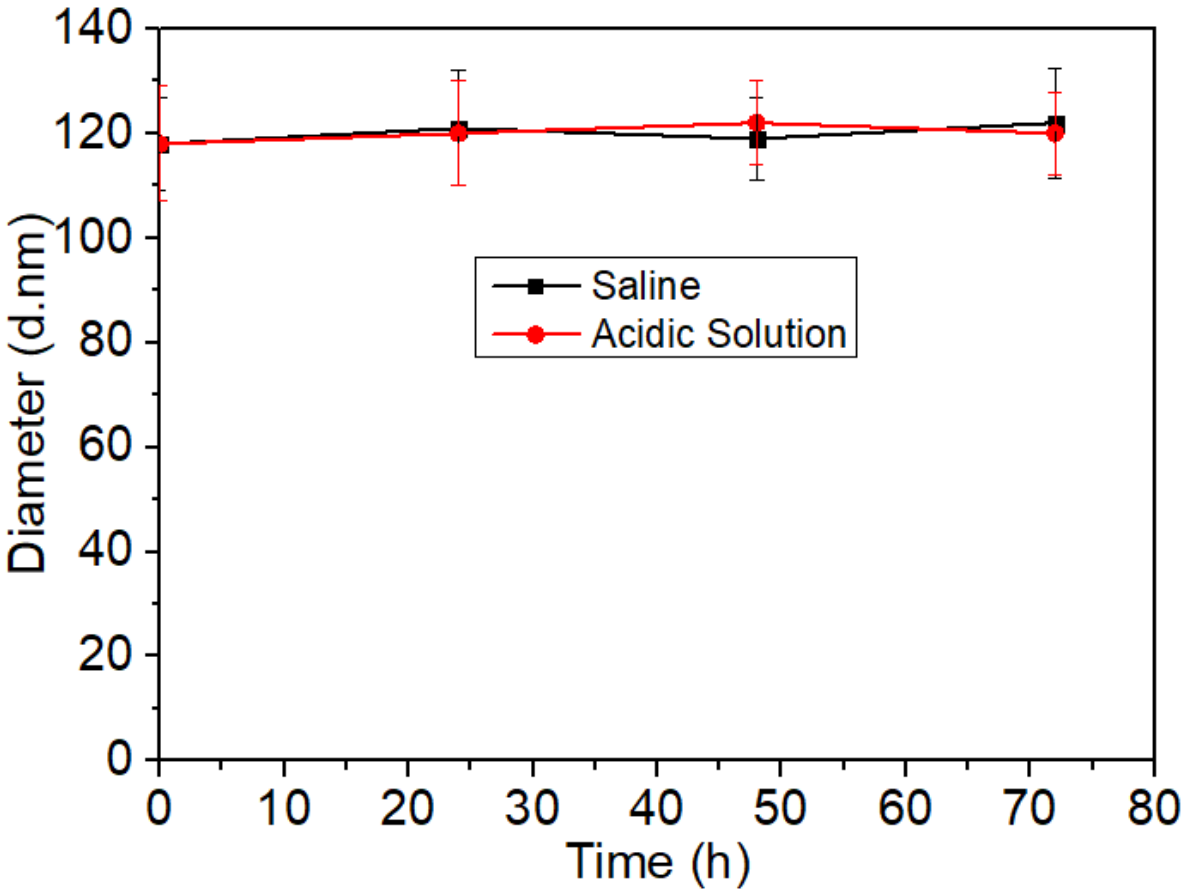

Figure S2. The hydrodynamic diameter of MPBZs in saline or acidic solutions of pH 1 at various times.

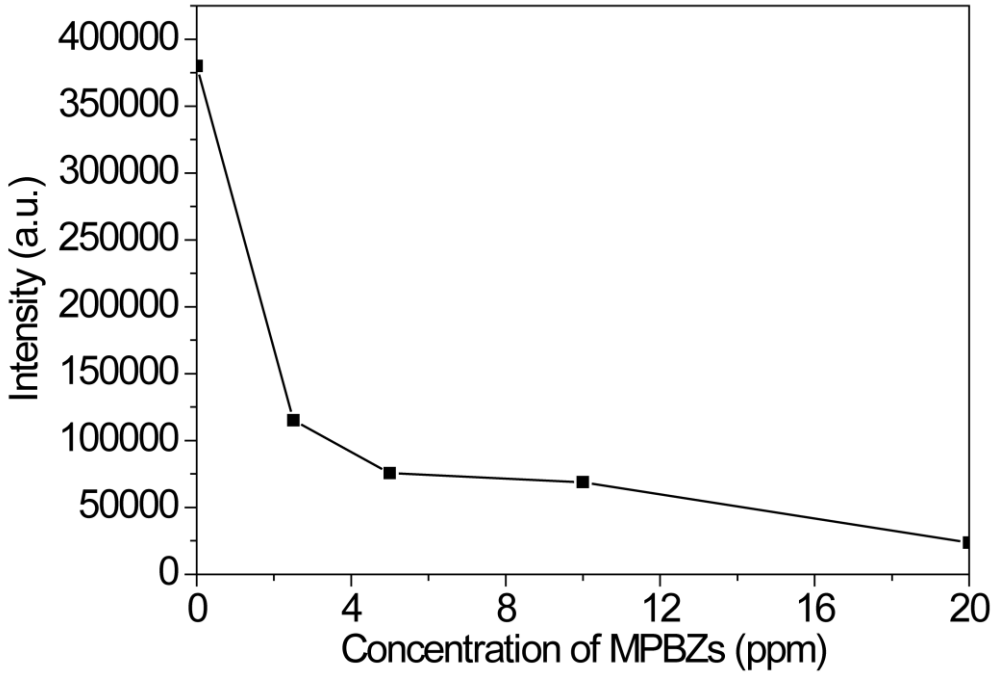

Figure S3. The curve of the corresponding second peak intensity of BMPO/•OH. A typical ESR spectrum with a 1:2:2:1 intensity was obtained. Under UV irradiation (340 nm), commercial TiO_2 powders generate •OH. MPBZs at various concentrations (0, 2.5, 5, 10, and 20 mg/L) were added to 0.1 mg/mL TiO_2 and 50 mM BMPO in quartz capillary tubes, and then placed in the ESR cavity after UV irradiation or no treatment.

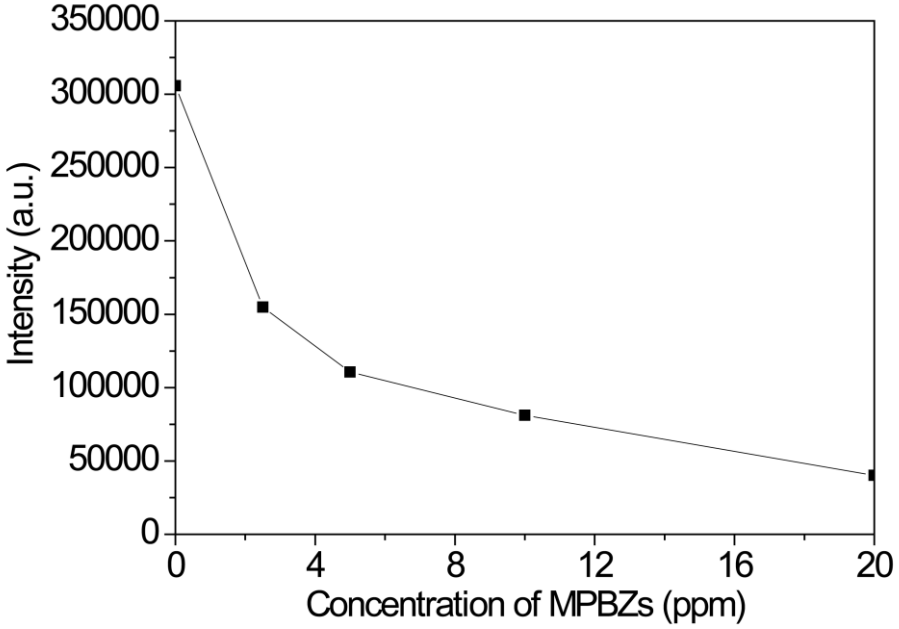

Figure S4. The curve of the corresponding second peak intensity of BMPO/•OOH. BMPO (5-tert-butoxycarbonyl 5-methyl-1-pyrroline-N-oxide) was selected as the $O_2^{\cdot-}$ trapping agent. MPBZs at various concentrations (0, 2.5, 5, 10, and 20 mg/L) were added into the xanthine and XOD system before an electron spin resonance test.

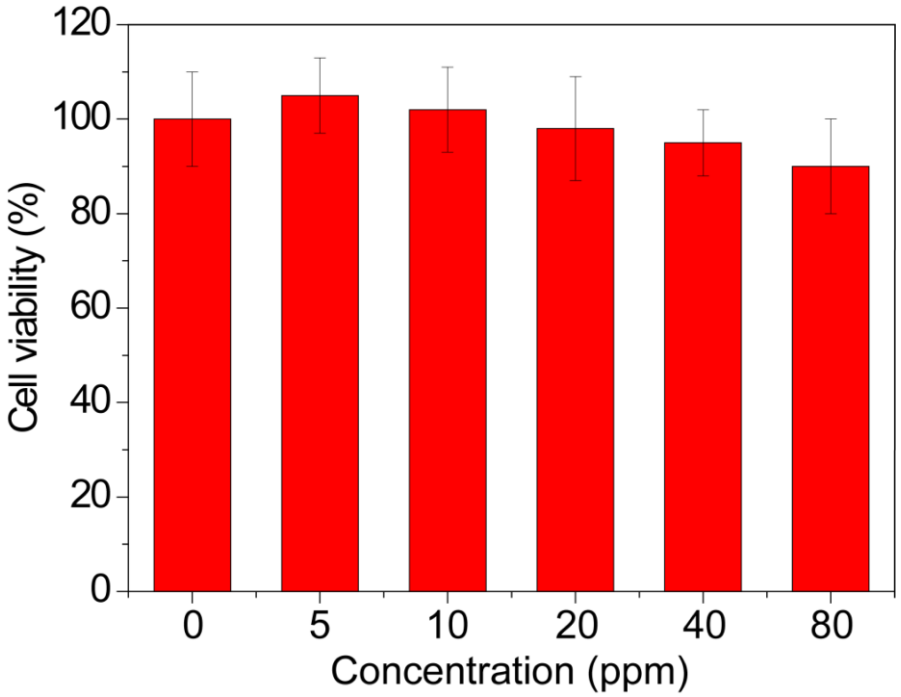

Figure S5. The cell viability of MPBZs with various concentrations.

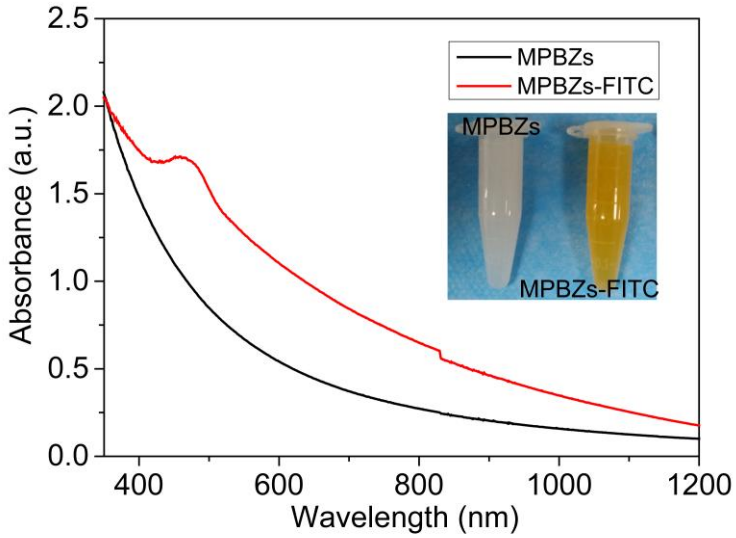

Figure S6. The UV-vis-NIR spectra of MPBZs before and after mixing with FITC.

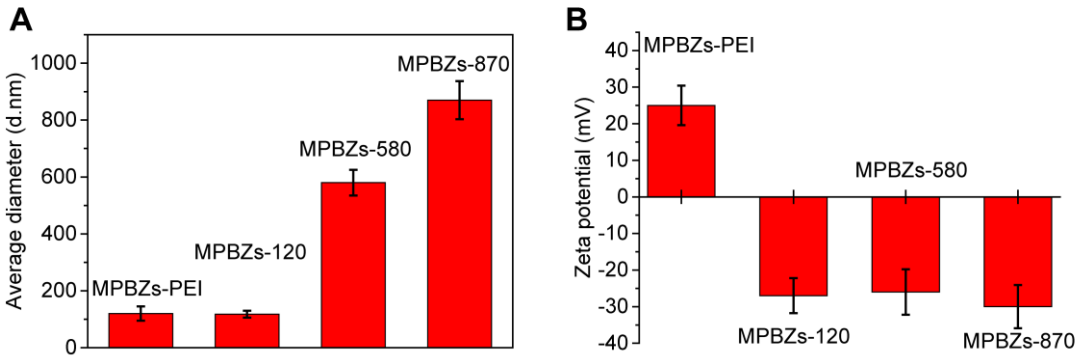

Figure S7. (a) The average hydrodynamic diameter and (b) zeta potential of four kinds of MPBZs with different size and surface charges.

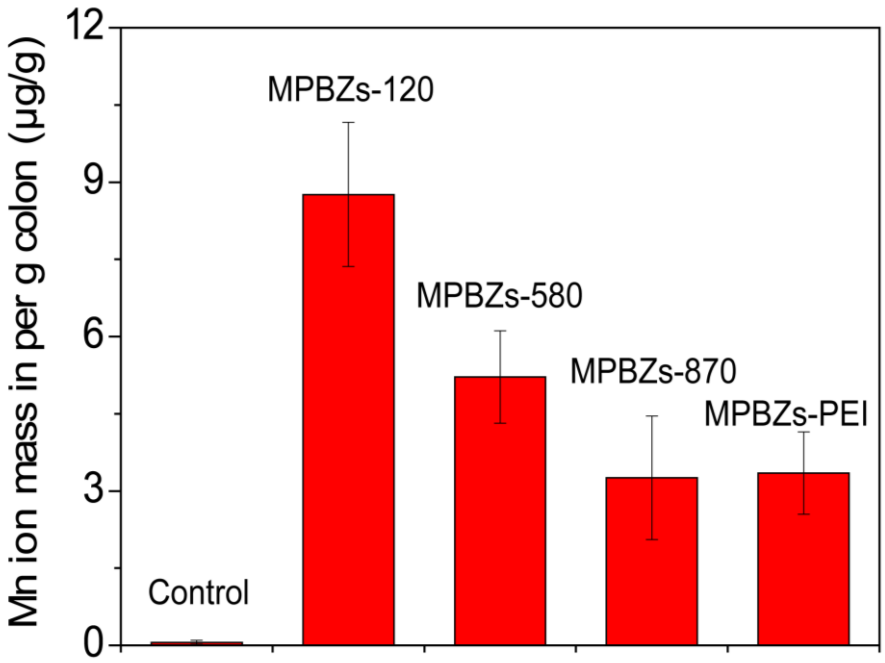

Figure S8. The accumulation of MPBZs at the inflamed mucosa among were investigated. Four kinds of MPBZs of different sizes and surface charges (the average hydrodynamic diameters of MPBZs with negative surface charges: 120 nm, 580 nm, and 870 nm; the average hydrodynamic diameter of MPBZs with positive surface charges: 118 nm.

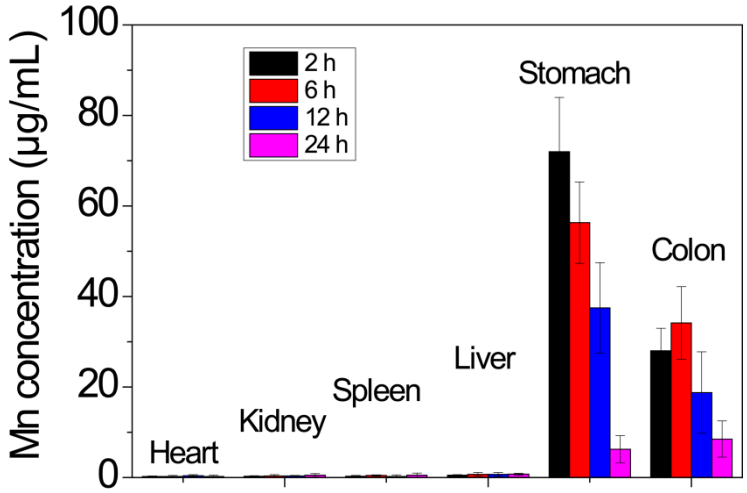

Figure S9. The distribution of MPBZs in IBD mice measured by ICP-OES.

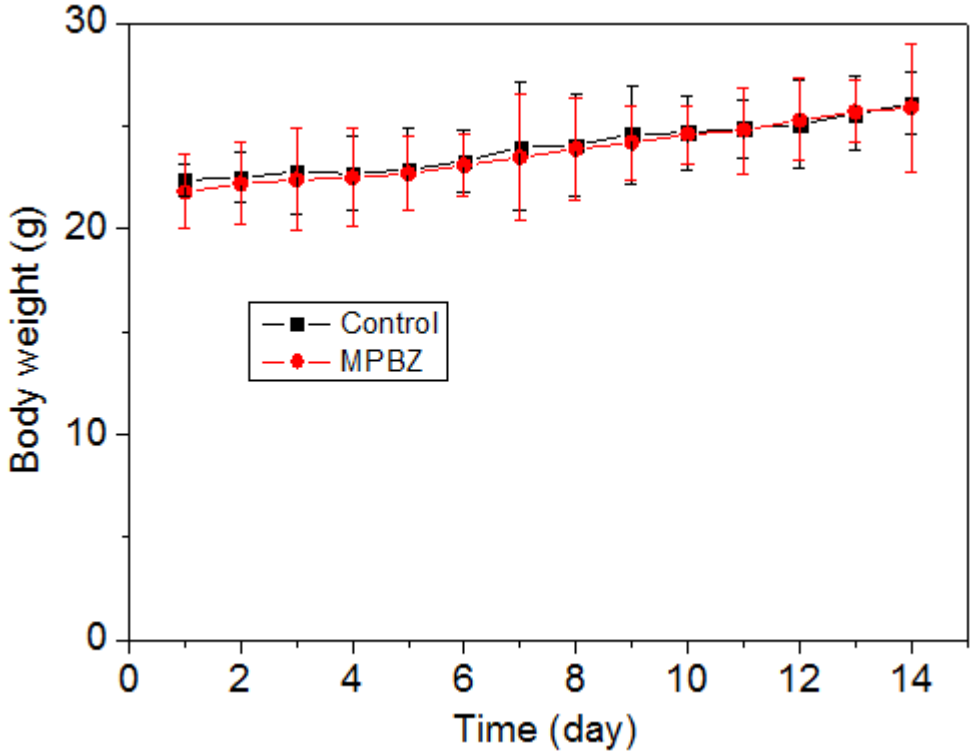

Figure S10. The body weight change of mice in control group and MPBZ-treated group.

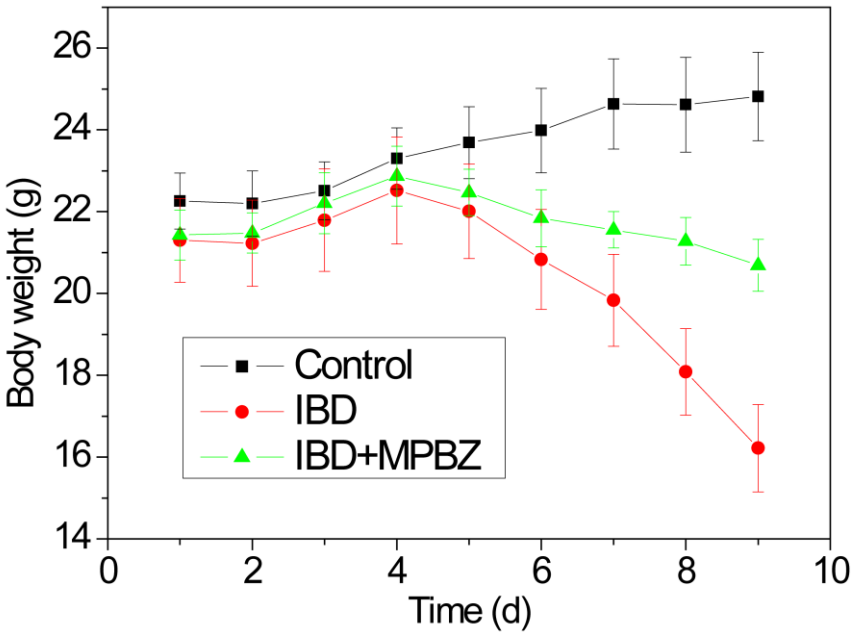

Figure S11. The body weight change of mice in various groups (Control, IBD, and IBD+MPBZ).

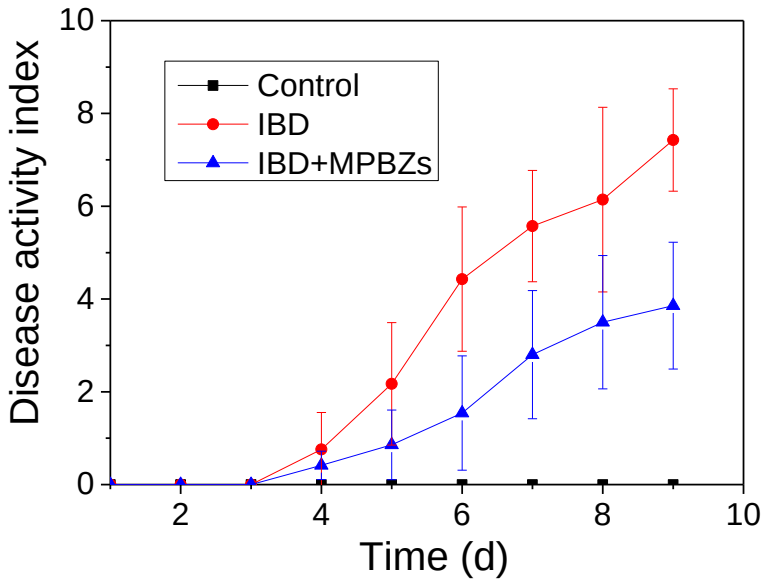

Figure S12. Changes of DAI of mice in various groups.

Figure S13. The images of colons of mice in various groups (Control, IBD, and IBD+MPBZs).

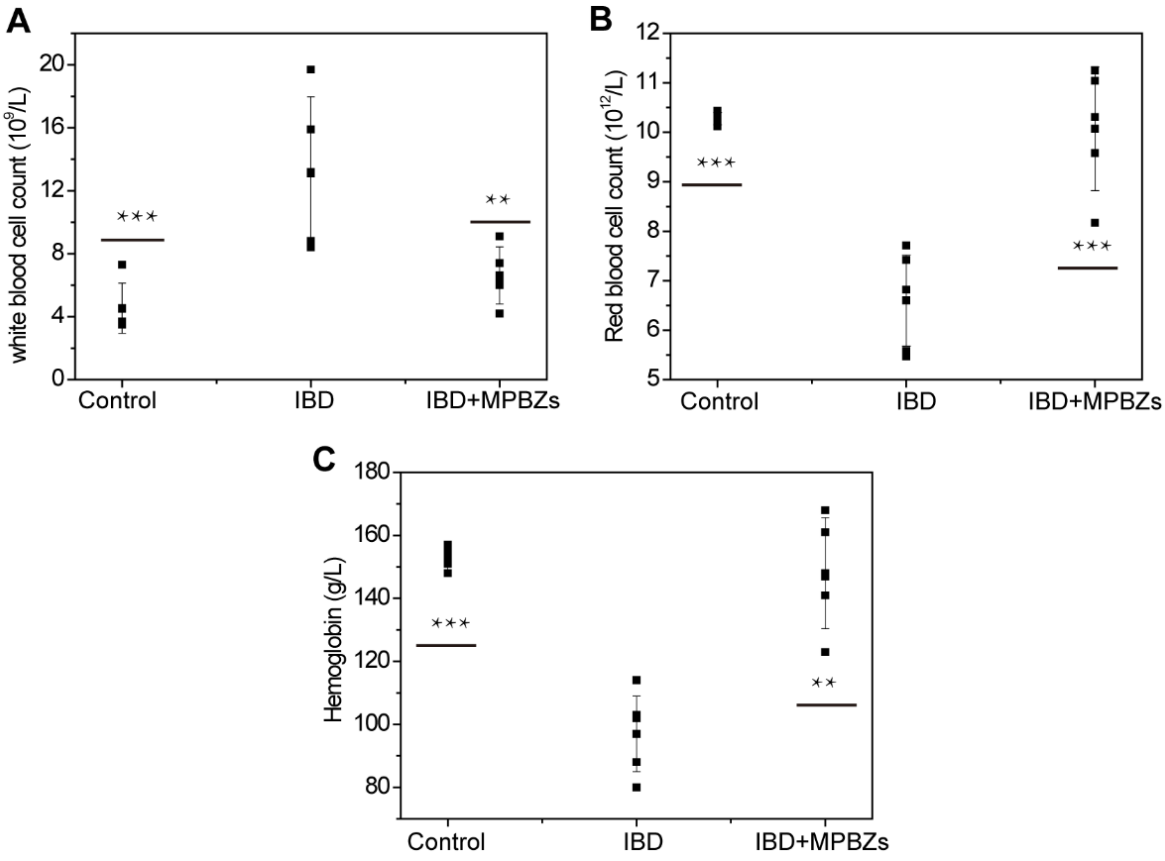

Figure S14. (a) white blood cell, (b) red blood cell, (c)Hematologic analyses including of mice from various groups (Control, IBD, and IBD+MPBZs).

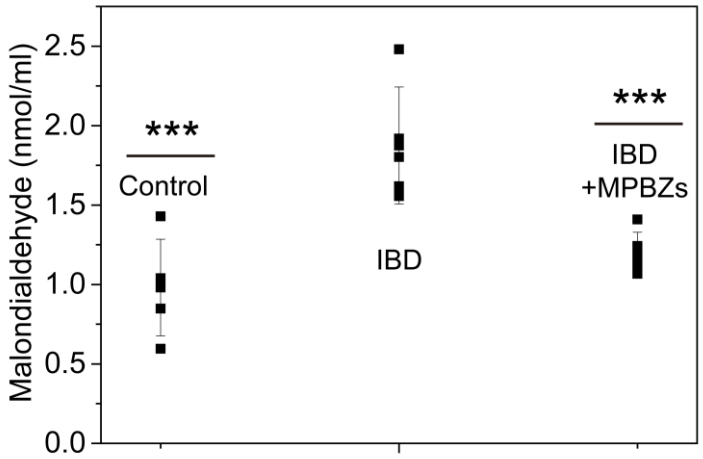

Figure S15. The levels of MDA activity in various groups (Control, IBD, and IBD+MPBZs).

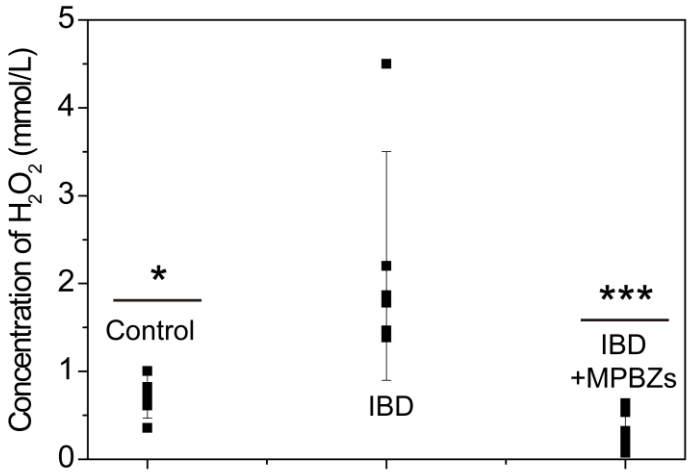

Figure S16. The intensity of H_2O_2 in various groups (Control, IBD, and IBD+MPBZs).. The intensity of hydrogen peroxide in mice with colitis was 2.20±0.58 mmol/L, higher than that in control mice (0.71±0.11 mmol/L), and was markedly reduced in the MPBZ-treated group (0.32±0.11 mmol/L).

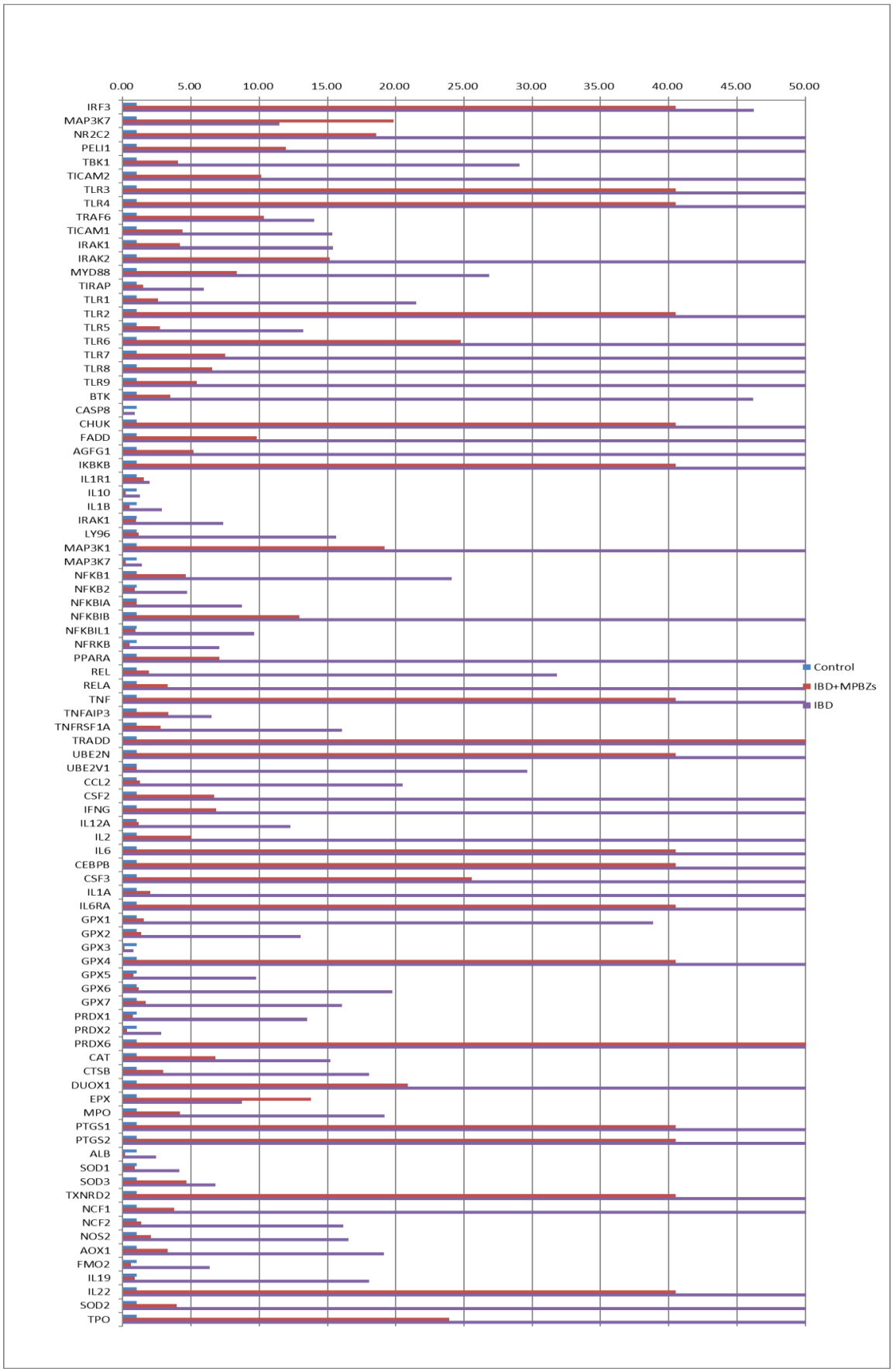

Figure S17. Cytokine profiles from a multiplexed cytokine assay of mice in the various groups (Control, IBD, and IBD+MPBZs).

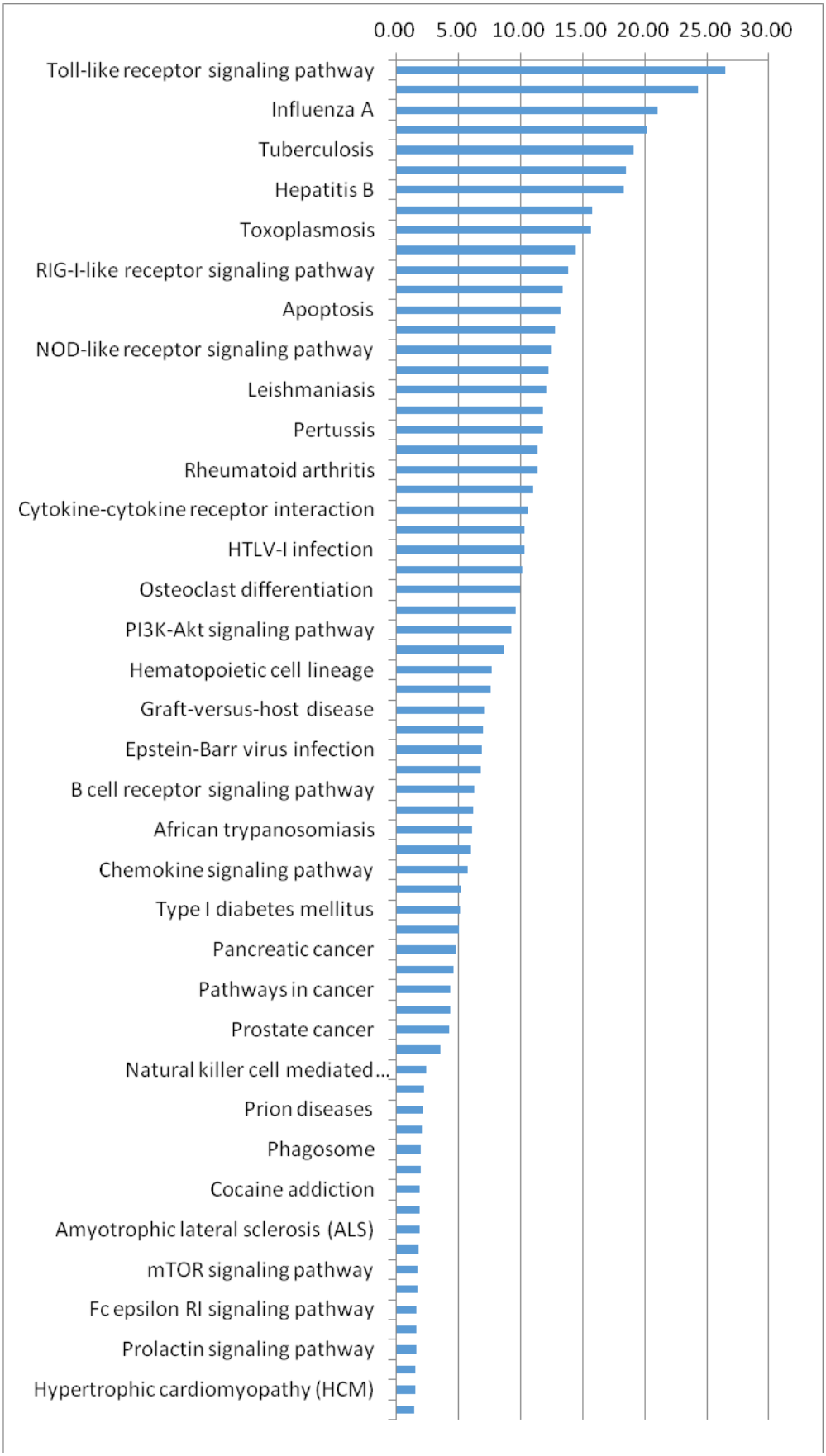

Figure S18. The KEGG pathway analysis of MPBZs on the DSS-induced colitis mice.

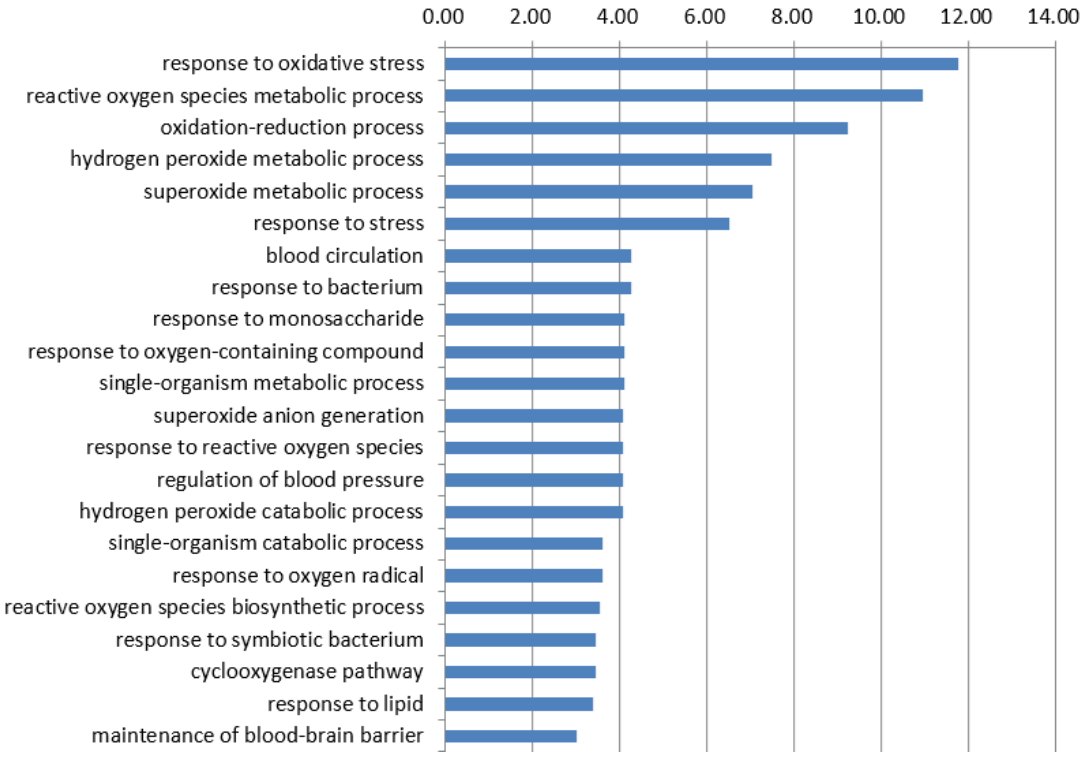

Figure S19. The GO analysis signaling pathway of MPBZs on the DSS-induced colitis mice.

Number	Gene Name	RefSeq
1	IRF3	NM_016849.4
2	MAP3K7	NM_009316.1
3	NR2C2	NM_001347342.1
4	PELI1	NM_023324.2
5	TBK1	NM_019786.4
6	TICAM2	NM_173394.3
7	TLR3	NM_126166.4
8	TLR4	NM_021297.2
9	TRAF6	NM_009424.3
10	TICAM1	NM_174989.4
11	IRAK1	NM_001177973.1
12	IRAK2	NM_001113553.1
13	MYD88	NM_010851.2
14	TIRAP	NM_001177845.1
15	TLR1	NM_030682.1
16	TLR2	NM_011905.3
17	TLR5	NM_016928.2
18	TLR6	NM_011604.3
19	TLR7	NM_133211.3
20	TLR8	NM_133212.2
21	TLR9	NM_031178.2
22	BTK	NM_013482.2
23	CASP8	NM_009812
24	CHUK	NM_001162410.1
25	FADD	NM_010175.5
26	AGFG1	NM_001310713.1
27	IKBKB	NM_001159774.1
28	IL1R1	NM_001123382.1
29	IL10	NM_010548.2
30	IL1B	NM_008361.3
31	IRAK1	NM_001177973.1
32	LY96	NM_001159711.1
33	MAP3K1	NM_011945.2
34	MAP3K7	NM_009316.1
35	NFκB1	NM_008689.2
36	NFκB2	NM_001177369.1
37	NFκBIA	NM_001105720.2
38	NFκBIB	NM_001306222.1
39	NFκBIL1	NM_010909.4
40	NFRκB	NM_172766.3
41	PPARA	NM_001113418.1
42	REL	NM_009044.2
43	RELA	NM_009045.4
44	TNF	NM_013693.2
45	TNFAIP3	NM_001166402.1
46	TNFRSF1A	NM_011609.4
47	TRADD	NM_001033161.2

48	UBE2N	NM_080560.3
49	UBE2V1	NM_001311131.1
50	CCL2	NM_011333.3
51	CSF2	NM_009969.4
52	IFNG	NM_008337.3
53	IL12A	NM_001159424.1
54	IL2	NM_008366.3
55	IL6	NM_031168.1
56	CEBPB	NM_024125.4
57	CSF3	NM_009971.1
58	IL1A	NM_010554.4
59	IL6RA	NM_001310676.1
60	GPX1	NM_008160.6
61	GPX2	NM_030677.2
62	GPX3	NM_008161.3
63	GPX4	NM_001037741.3
64	GPX5	NM_010343.2
65	GPX6	NM_145451.3
66	GPX7	NM_024198.3
67	PRDX1	NM_011034.4
68	PRDX2	NM_011563.5
69	PRDX6	NM_007453.3
70	CAT	NM_012520.1
71	CTSB	NM_007798.3
72	DUOX1	NM_001099297.1
73	EPX	NM_007946.2
74	MPO	NM_010824.2
75	PTGS1	NM_008969.4
76	PTGS2	NM_011198.3
77	ALB	NM_009654.4
78	SOD1	NM_011434.1
79	SOD3	NM_011435.3
80	TXNRD2	NM_013711.3
81	NCF1	NM_001286037.1
82	NCF2	NM_010877.5
83	NOS2	NM_010927.3
84	AOX1	NM_009676.2
85	FMO2	NM_018881.3
86	IL19	NM_001009940.1
87	IL22	NM_016971.2
88	SOD2	NM_013671.3
89	TPO	NM_009417.2
90	β-actin	NM_007393.5

Table S1. The Names and Reference Sequence (Ref Seq) from National Center for Biotechnology Information (NCBI) of target genes in inflammation-related and oxidation-related signaling pathways.

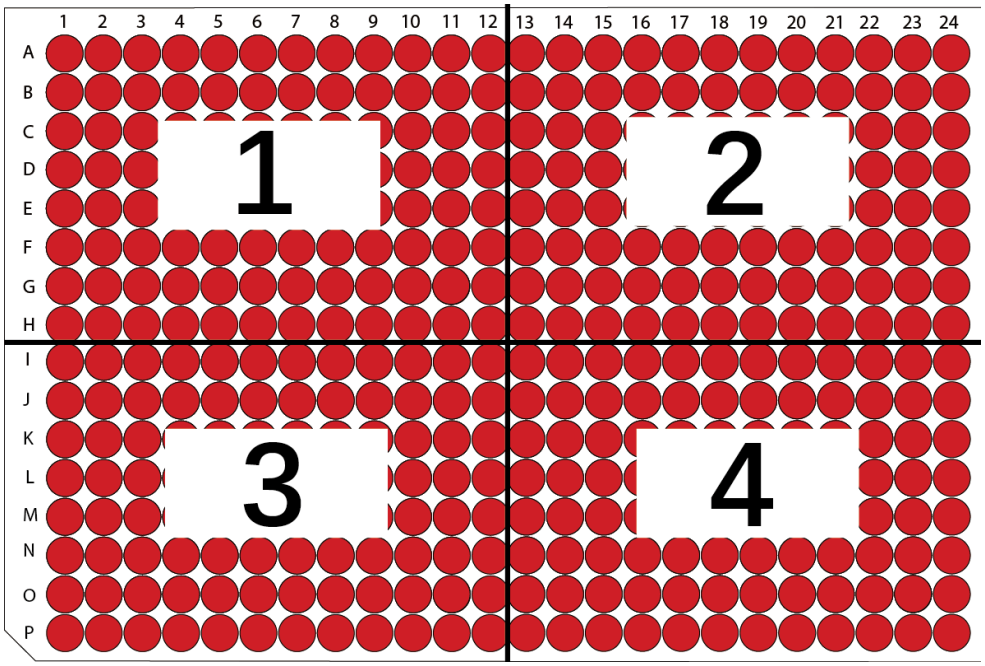

Scheme S1: PCR Array Diagram